

Supporting information

Scalable fabrication of ultra-fine lithiophilic nanoparticles encapsulated in soft buffered hosts for long-life anode-free Li₂S-based cells

Bo Zhou^{a,d}, Ting Li^a, Anjun Hu^{a,b*}, Baihai Li^e, Runjing Li^a, Chuan Zhao^a, Nian Chen^{c,*}, Miao He^b, Jing Liu^a, Jianping Long^{a*}

^a College of Materials and Chemistry & Chemical Engineering, Chengdu University of Technology,
1#, Dongsanlu, Erxianqiao, Chengdu 610059, Sichuan, China

^b State Key Laboratory of Electronic Thin Film and Integrated Devices, University of Electronic
Science and Technology of China, Chengdu 610054, China

^c The First Affiliated Hospital, Department of Medical Cosmetic, Hengyang Medical School,
University of South China, Hengyang, Hunan, 421001, China

^d Zhangjiajie Institute of Aeronautical Engineering, 1#, xueyuan Rd, Wulingshan Avenue, Zhangjiajie
427000, Hunan, China

^e School of Materials and Energy, University of Electronic Science and Technology of China,
Chengdu 610054, China

* Corresponding author: *anjunhu@feishu.uestc.cn* (Anjun Hu); *chenniangood@126.com* (Nian Chen);
longjianping@cdut.cn (Jianping Long)

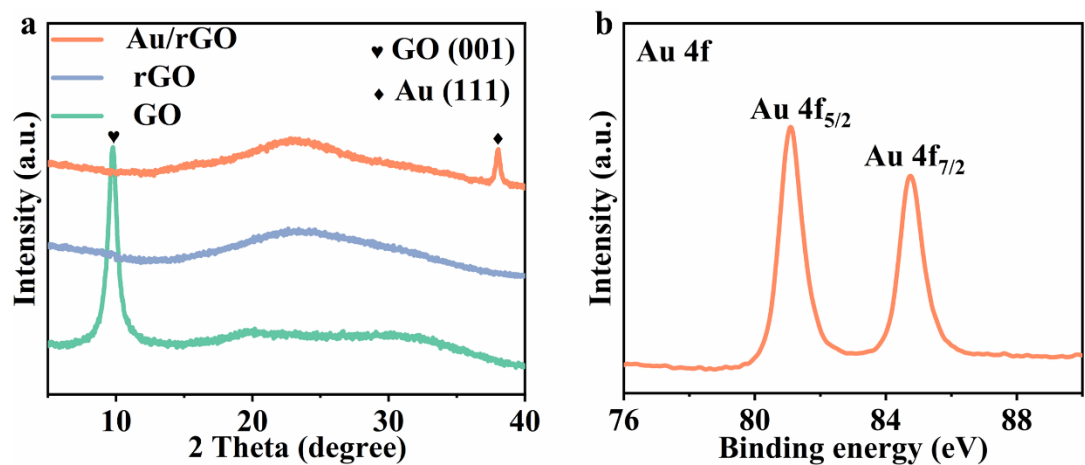


Fig. S1 (a) XRD of the pristine GO and rGO and Au/rGO film and (b) XPS spectra of Au/rGO film.

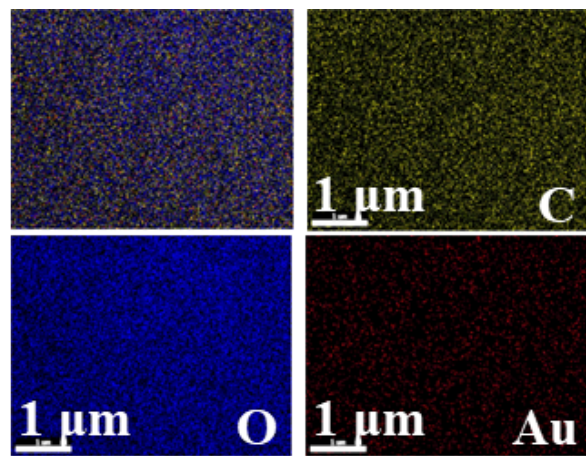


Fig. S2 EDX mapping of the C, O, and Au elements of Au/rGO film.

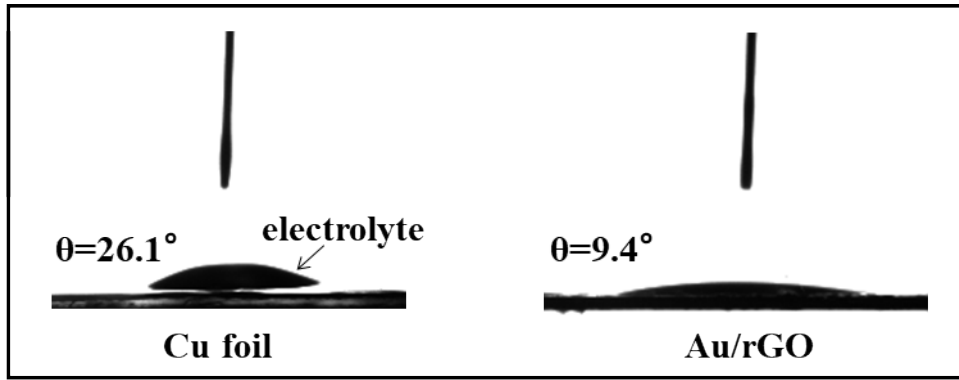


Fig. S3 Contact angles of electrolyte on pristine Cu foil and Au/rGO film.

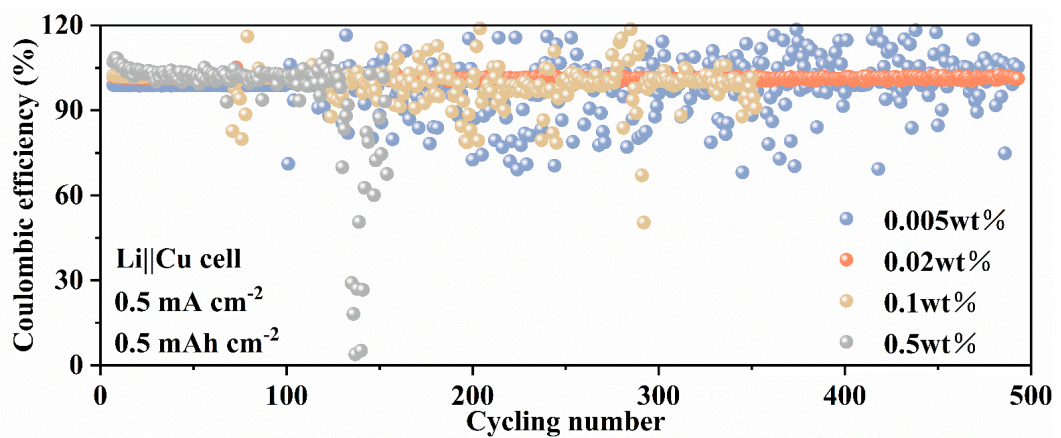


Fig. S4 Coulombic efficiencies of Au/rGO with different Au contents at $0.5 \text{ mA cm}^{-2}/0.5 \text{ mAh cm}^{-2}$.

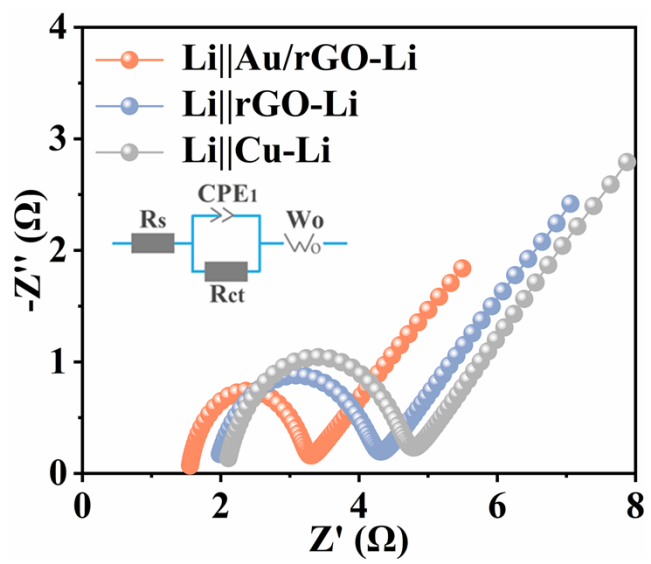


Fig. S5 Nyquist plots of $\text{Li}||\text{Cu}$, $\text{Li}||\text{rGO}$, and $\text{Li}||\text{Au/rGO-Li}$ cells after 50 cycles at $2 \text{ mA cm}^{-2}/2 \text{ mAh cm}^{-2}$.

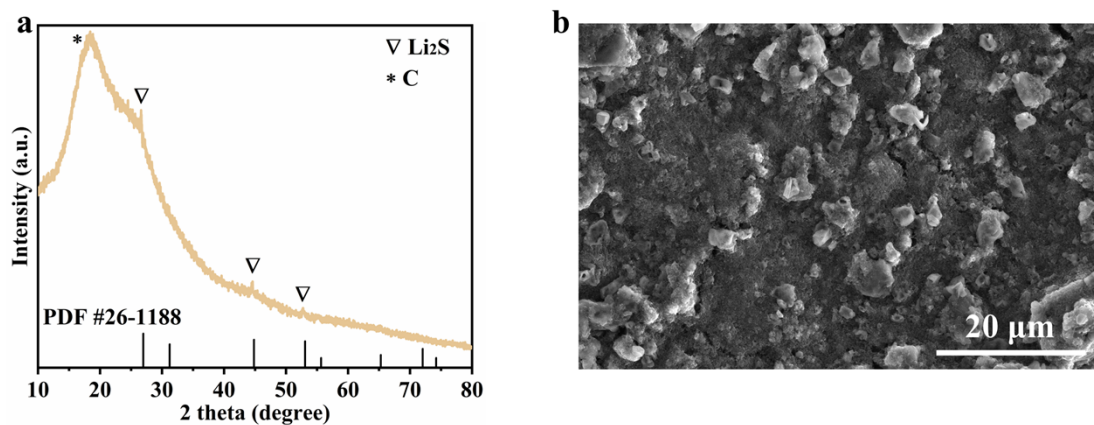


Fig. S6 (a) XRD pattern of the Li₂S/C cathode and (b) SEM image.

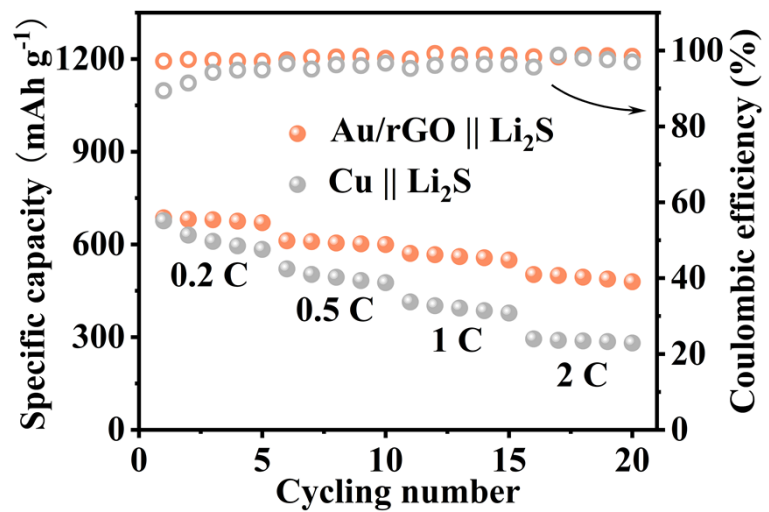


Figure S7 Rate performance of Au/rGO||Li₂S and Cu||Li₂S.

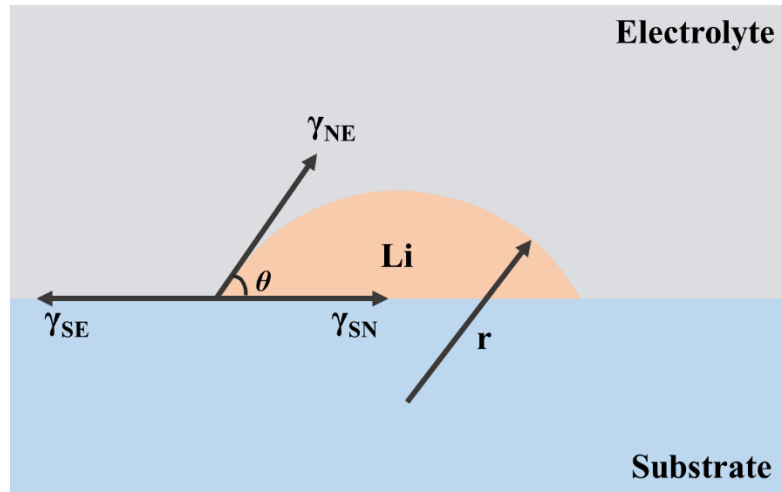


Fig. S8 Schematic representation of the Li nucleation on substrate based on the classical heterogeneous nucleation model.

Note 1: According to classical heterogeneous nucleation theory, the critical nucleation radius (r^*) is determined by

$$r^* = 2\gamma_{NE} / \Delta G_V$$

where ΔG_V is the free energy change of Li from electrolyte to anode and γ_{NE} is Li/electrolyte interfacial free energy. The r^* is unaffected by the substrate. However, the volume of nucleated Li to reach r^* is much smaller than that in homogeneous nucleation, indicating the important role of substrate in regulating Li nucleation.

Li heterogeneous nucleation barrier is related to the binding energy (E_b) between the substrate and Li.

$$\Delta G_{het} = S(\theta) \Delta G_{hom}$$

$$S(\theta) = (2 + \cos\theta) (1 - \cos\theta)^2 / 4$$

$$\cos\theta = (\gamma_{SE} - \gamma_{SN}) / \gamma_{NE}$$

Where ΔG_{het} and ΔG_{hom} are the heterogeneous and homogeneous nucleation barrier, respectively. θ is contact angle, γ_{SE} , γ_{SN} , and γ_{NE} are the interfacial free energy of substrate-electrolyte, substrate-nucleus, and nucleus-electrolyte interfacial free energy, respectively.

When the E_b between Li and substrate is increased, γ_{SN} is reduced. Therefore, $\cos\theta$ is increased and $S(\theta)$ as well as ΔG_{het} is decreased. In summary, substrates that can provide a high E_b toward Li can reduce the Li nucleation barrier as well as the volume of nucleated Li to reach r^* , favoring uniform Li deposition.^{1, 2} The E_b is thus a reasonable descriptor of the lithiophilicity of anodic substrates.

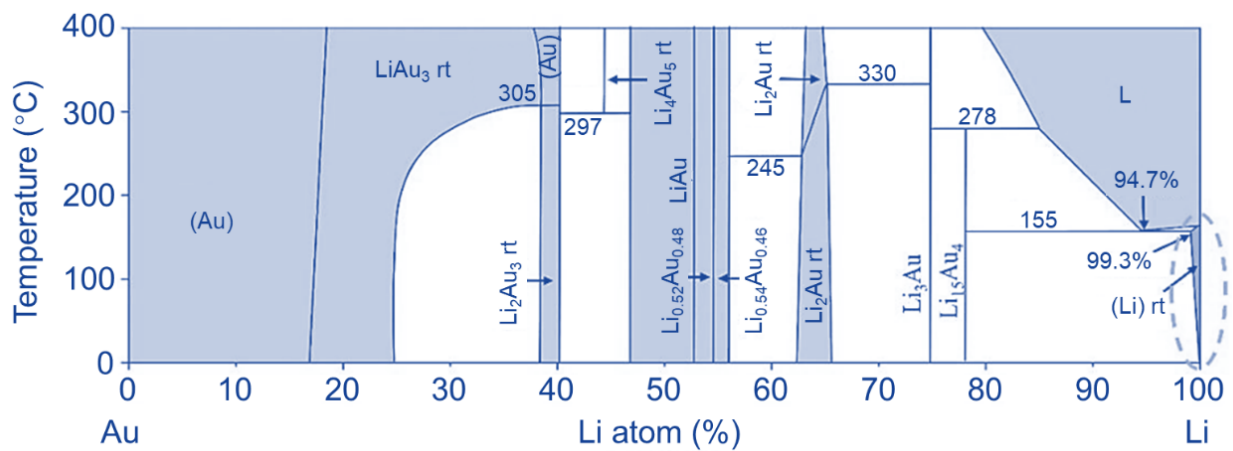


Fig. S9 Phase diagrams of Li–Au.³

Table S1. Comparison of main parameters and cycling property for this work with recently reported anode-free full cell.

Battery system	Initial discharge capacity (mA h g ⁻¹)	Cycle life	Capacity retention	Current density	Reference
Cu Li ₂ S	639	100	51.5 %	0.1 C	⁴
Cu LiNi _{0.5} Mn _{0.3} Co _{0.2} O ₂	162	100	42 %	0.1 C	⁵
Cu@PEO LiFePO ₄	127	100	49.6 %	0.2 C	⁶
3D-Cu Li ₂ S	588.4	180	59.34 %	0.1 C	⁷
MLG LiFePO ₄	151	100	61 %	0.1 C	⁸
15Ph5 LiFePO ₄	106.9	100	63 %	0.2 C	⁹
Au/rGO Li ₂ S	673.1	200	63.3 %	0.2 C	This work

Table S2. The calculation of the energy density of the Au/rGO||Li₂S anode-free full cell in our work.

Components	value
Li ₂ S mass loading (mg cm ⁻²)	2.0
Area of the electrode film (cm ²)	1.131
The mass of Li ₂ S (mg)	2.262
The mass of carbon black (mg)	0.97
The mass of PVDF (mg)	0.36
The mass of current collector (cathode, mg)	4.95
The mass of the whole cathode (mg)	8.542
The mass of Au (mg)	0.00006
The mass of rGO current collector (mg)	0.30531
The mass of the whole anode (mg)	0.3054
Total mass (mg)	8.8474
The initial discharge capacity (mAh g ⁻¹)	673.1

According table S2, the gravimetric energy density can be calculated as below. The mass of electrolyte and packing materials are not included.¹⁰

$$M_{\text{Gravimetric energy density}} = \frac{E \times Q_{\text{Li}_2\text{S}} \times m_{\text{Li}_2\text{S}}}{m_{\text{total}}}$$
$$= \frac{2.1 \times 673.1 \times 3.232}{8.8474} \text{ Wh kg}^{-1}$$
$$\approx 516.4 \text{ Wh kg}^{-1}$$

E is the average discharge voltage of the full cell, Q_{Li₂S} is the theoretical gravimetric specific capacities of Li₂S cathode, m_{Li₂S} is the mass of Li₂S cathode.

Table S3. The material cost of various components¹⁰.

Category	Price (\$ g ⁻¹)	Unit area consumption (mg cm ⁻²)	Unit area cost (\$ cm ⁻²)
Li ₂ S*	30.02	2	6.0×10 ⁻²
Au**	47	0.000054	2.54×10 ⁻⁶
rGO*	79.81	0.27	2.15×10 ⁻²
Al foil***	/	/	0.16
Carbon black****	0.07	0.857	0.6×10 ⁻⁴
PVDF****	0.215	0.318	0.68×10 ⁻⁴

* The price of rGO and Li₂S are from Shanghai Aladdin Biochemical Technology Co., Ltd.

** The prices of Au are from the website of <https://www.ccmn.cn>.

*** The prices of Al foil are from Shenzhen Kejing Microelectronics Technology Co., Ltd.

****Suzhou Duoduo Chemical Technology Co., Ltd.

The theoretical cost of the Au@rGO||Li₂S anode-free full

$$\text{cell}=1.131 \times (6.0 \times 10^{-2} + 2.54 \times 10^{-6} + 2.15 \times 10^{-2} + 0.16 + 0.6 \times 10^{-4} + 0.68 \times 10^{-4}) / (673.1 \times 10^{-3}) = 0.41 \text{ \$ Ah}^{-1}$$

- 1 H. Zhang, X. Liao, Y. Guan, Y. Xiang, M. Li, W. Zhang, X. Zhu, H. Ming, L. Lu, J. Qiu, Y. Huang, G. Cao, Y. Yang, L. Mai, Y. Zhao, H. Zhang, *Nat. Commun.*, 2018, **9**, 3729. <https://doi.org/10.1038/s41467-018-06126-z>.
- 2 Y.-X. Yao, X.-Q. Zhang, B.-Q. Li, C. Yan, P.-Y. Chen, J.-Q. Huang, Q. Zhang, *InfoMat*, 2020, **2**, 379-388. <https://doi.org/10.1002/inf2.12046>.
- 3 K. Yan, Z. Lu, H.-W. Lee, F. Xiong, P.-C. Hsu, Y. Li, J. Zhao, S. Chu, Y. Cui, *Nat. Energy*, 2016, **1**, 16010. <https://doi.org/10.1038/nenergy.2016.10>.
- 4 S. Nanda, A. Gupta, A. Manthiram, *Adv. Energy Mater.*, 2018, **8**, 1801556. <https://doi.org/10.1002/aenm.201801556>.
- 5 A. J. Louli, M. Genovese, R. Weber, S. G. Hames, E. R. Logan, J. R. Dahn, *J. Electrochem. Soc.*, 2019, **166**, A1291-A1299. <https://doi.org/10.1149/2.0091908jes>.
- 6 A. A. Assegie, J. H. Cheng, L. M. Kuo, W. N. Su, B. J. Hwang, *Nanoscale*, 2018, **10**, 6125-6138. <https://doi.org/10.1039/C7NR09058G>.
- 7 H. Cheng, C. Gao, N. Cai, M. Wang, *Chem. Commun.*, 2021, **57**, 3708-3711. <https://doi.org/10.1039/d1cc00006c>.
- 8 A. A. Assegie, C.-C. Chung, M.-C. Tsai, W.-N. Su, C.-W. Chen, B.-J. Hwang, *Nanoscale*, 2019, **11**, 2710-2720. <https://doi.org/10.1039/C8NR06980H>.
- 9 J. Lee, Y.-G. Cho, D. Gu, S. Kim, *ACS Appl. Mater. Interfaces*, 2022, **14**, 15080-15089. <https://doi.org/10.1021/acsami.1c21183>.
- 10 J. Chen, J. Xiang, X. Chen, L. Yuan, Z. Li, Y. Huang, *Energy Storage Mater.*, 2020, **30**, 179-186. <https://doi.org/10.1016/j.ensm.2020.05.009>.